This peer-reviewed published paper appears as: Elkady, A. and Lignos, D. G. (2018). "Improved Seismic Design and Nonlinear Modeling Recommendations for Wide-Flange Steel Columns". *ASCE Journal of Structural Engineering 144(9)*. DOI: 10.1061/(ASCE)ST.1943-541X.0002166

Improved Seismic Design and Nonlinear Modeling Recommendations for Wide-Flange Steel Columns

Ahmed Elkady, Ph.D.[1] and Dimitrios G. Lignos, M.ASCE[2]

Abstract: This paper presents the findings of parametric finite element (FE) simulations of more than 50 wide-flange steel columns under cyclic loading. The column sizes, which are mostly highly ductile according to the current design practice in North America, are those seen in new and existing steel seismic-resistant moment frames. The parametric study is based on a high-fidelity FE model, which is thoroughly validated with available full-scale steel column experimental data. In the FE simulations, variations in the employed lateral loading history, the applied axial load ratio were considered to assess and refine a number of provisions related to the seismic design of steel MRF columns. The assessment is based on a number of performance indicators including the column axial shortening and corresponding plastic hinge length, the column plastic rotation capacity influenced by local and global geometric instabilities, as well as the lateral stability bracing force demands. Empirical expressions are proposed to estimate these performance indicators as a function of geometric and loading parameters. Based on these expressions, seismic design recommendations are proposed to maintain column stability. A comparison with the current ASCE 41-13 nonlinear modeling provisions for steel columns is also made and specific recommendations are proposed to update the limits for force-controlled wide-flange steel columns.

Keywords: Steel columns; finite element modeling; loading history; column axial shortening; out-of-plane brace force; plastic hinge length; ASCE 41.

[1] Post-doctoral Research Scientist, Swiss Federal Institute of Technology, Lausanne (EPFL), Switzerland
[2] Associate Professor, Swiss Federal Institute of Technology, Lausanne (EPFL), Switzerland

Introduction

The use of steel moment-resisting frames (MRFs) in seismic zones is well established. In steel MRFs, the steel beams are expected to dissipate the seismic energy through flexural yielding. Although steel columns should remain elastic due to the employed capacity design principles (i.e., strong-column/weak-beam ratio), flexural yielding is still permitted near the column base. Lignos et al. (2016) gathered all the available experimental data on wide-flange steel columns published to date (Popov et al. 1975; MacRae et al. 1990; Nakashima et al. 1990; Newell and Uang 2006; Cheng et al. 2013; Chen et al. 2014; Suzuki and Lignos 2015; Lignos et al. 2016; Ozkula et al. 2017; Elkady and Lignos 2018), which comprised of 155 specimens in total. The majority of them satisfy the web compactness limit for highly ductile members, λ_{hd}, as per ANSI/AISC 341-16 (AISC 2016a). This is shown in Fig. 1a that summarizes the range of applied axial load ratios, P/P_{CL} [P is the applied load and P_{CL} is the lower-bound compressive strength calculated as per ASCE (2014)], with respect to the local web slenderness ratio, h/t_w, of the gathered column specimen cross-sections. The experimental data suggests that steel columns utilizing stocky cross-sections (i.e., $7.6 < h/t_w < 17$, $3.1 < b_f/2t_f < 5$) exhibit a very stable hysteretic behavior without practically experiencing cyclic and/or in-cycle flexural strength deterioration. This is illustrated in Fig. 1b that shows the column rotation capacity, θ_{max} at the peak response (i.e., prior to onset of local buckling), with respect to h/t_w. On the other hand, the hysteretic behavior of deep and slender cross-sections (i.e., $30 < h/t_w < 50$, $5 < b_f/2t_f < 7$) may be significantly compromised due to the coupling of local and member geometric instabilities at 2%-3% lateral drift demands. Referring to Fig. 1c, this is not necessarily the case if the axial load demands vary due to dynamic overturning effects, which is typical in end (i.e., exterior) columns (Suzuki and Lignos 2015). The gathered experiments also suggest that the plastic deformation capacity of highly ductile steel columns is appreciable even in cases that P/P_{CL} > 0.50 (see Fig. 1c). This implies that the current limit for force-controlled elements as per ASCE/SEI 41-13 (ASCE 2014) may be overly conservative. The aforementioned concerns have also been raised by engineering practitioners (Bech et al. 2015; Hamburger et al. 2016).

The prior testing programs provide valuable insights into the behavior of steel wide-flange columns subjected to cyclic loading. Given the limited range of test parameters (e.g., specimen geometry, applied loading schemes, etc.), the above observations cannot be fully generalized such that the current seismic design and modeling recommendations for wide-flange steel columns can be assessed and further improved. Therefore, the above experimental database should be complemented with additional finite element simulations. Few prior studies have been conducted in this direction (Elkady and Lignos 2012, 2015a; Stoakes and Fahnestock 2016; Fogarty et al. 2017). However, several issues that influence the steel column stability under seismic loading have not been fully addressed. These include the column axial shortening, the column plastic hinge length, the employed loading history as well as the steel column stability bracing force demands.

This paper fulfills all purposes. In particular, a continuum FE modeling approach is first proposed to simulate the behavior of steel columns subject to cyclic loading. This approach is validated with past experiments on wide-flange steel columns under multi-axis cyclic loading. Through parametric simulations, the North American seismic design criteria (CSA 2009; AISC 2016b) for steel MRF columns are assessed. Additional design criteria, related to column stability, are proposed. The gathered experimental data complemented with finite element simulations are also utilized to assess the current nonlinear modeling guidelines for the seismic evaluation of new and existing steel MRFs (ASCE 2014).

Proposed Finite Element Modeling Approach

A detailed FE modeling approach is proposed to simulate the hysteretic behavior of wide-flange steel columns subject to multi-axis cyclic loading. The commercial software ABAQUS-FEA/CAE (2011) is employed for this purpose. Referring to Fig. 2a, the proposed FE model represents a typical first-story steel MRF column and its boundary conditions. From this figure, a fixed column base assumption is only valid if the flexibility of the column base connection is neglected (Kanvinde et al. 2012; Grilli et al. 2017; Inamasu et al. 2017). This issue deserves more attention but it is outside the scope of the present study. The in-plane rigidity of fully-restrained beam-to-column connections intersecting the column top end in steel MRFs is represented by a flexible elastic beam-column element. The flexural stiffness of this element is tuned such that the inflection point within the column is always located at 0.75 L (L is the column length) measured from the column base, prior to column yielding. This is the expected inflection point location in typical first-story steel MRF columns (Gupta and Krawinkler 1999; Zareian et al. 2010; Elkady and Lignos 2015b).

The proposed FE model incorporates large strain and deformation formulations, and utilizes quadratic 4-node doubly curved "S4R" shell elements that capture the local buckling initiation and progression by preventing shear locking and hourglass. The finite element mesh size is determined such that both the cross-section's flanges and web are divided in a minimum of 12 and 24 elements, respectively. This size ensures minimal computational effort without compromising the solution accuracy. The optimum mesh size was determined based on a preceding mesh sensitivity analysis discussed in Elkady (2016).

The material constitutive relationships are based on a von Mises yield surface "J_2 plasticity" (von Mises 1913) with a well-established combined isotropic/kinematic hardening law (Lemaitre and Chaboche 1990). The nonlinear kinematic and isotropic hardening parameters defined in Eqs. (1) and (2), respectively, are based on one backstress,

$$\dot{\alpha} = C\frac{1}{\sigma^{o}\big|_{0}}(\sigma - \alpha)\dot{\varepsilon}_{pl} - \gamma\alpha\dot{\varepsilon}_{pl} \tag{1}$$

$$\sigma^{o} = \sigma^{o}\big|_{0} + Q_{\infty}\left(1 - e^{-b\,\varepsilon_{pl}}\right) \tag{2}$$

in which, C is the initial kinematic hardening modulus, γ is the rate at which C decreases with respect to the cumulative plastic strain ε_{pl}, α is the backstress, $\sigma^{o}|_{0}$ is the equivalent yield stress at zero plastic strain (i.e. σ_{y}), Q_{∞} is the maximum change in the size of the yield surface and b is the rate at which the size of the yield surface changes as plastic deformation develops. For a standard A992 Gr. 50 (ASTM 2015) steel material (i.e., nominal yield stress, σ_{yn}=345MPa), the following values are recommended for the four material model parameters if one backstress is employed: C=3378MPa (490ksi), γ=20, Q_{∞}=90MPa (13ksi), and b=12. The parameters were obtained through calibrations with uniaxial monotonic and cyclic coupon test data for A992 Gr. 50 steel material (i.e., nominal yield stress, f_y=345MPa). The reader is referred to Suzuki and Lignos (2017) for characteristic stress-strain comparisons for typical steel materials including A992 Gr. 50 steel. The modulus of elasticity and the expected yield stress are taken as E=200000MPa (29000ksi) and σ_{ye}=380MPa (55ksi), respectively. These values comply with the ones used in Suzuki and Lignos (2015) for A992 Gr. 50 steel. The aforementioned parameters depend only on the respective steel material but not on the imposed loading history.

Local and global imperfections should be consistently introduced into the FE model such that local and member geometric instabilities can be properly traced. This can be achieved by scaling and superimposing proper buckling modes of the respective column. In particular, two types of imperfections are introduced in the FE model: (1) local web and flange imperfections (see Fig. 2b); and (2) global out-of-straightness imperfections (see Fig. 2c). The proposed magnitude of local web and flange geometric imperfections are $d/250$ and $b_f/250$, respectively. Global imperfections (i.e., out-of-plane out-of-straightness of the column) should be limited to $L/1500$. The aforementioned values are tuned to provide the best fit between the FE simulation results and the gathered experimental column database with emphasis on cross-sections with $30 < h/t_w < 50$ that are commonly used in steel MRFs. Because the magnitude of imperfections is strongly influenced by cooling after the hot-rolling process (Alpsten 1968 and Young 1971), it is likely that the imposed imperfections in stocky cross-sections ($h/t_w < 35$) may be larger but still less than the manufacturing limits as per ASTM (2003) (i.e., $b_f/150$ and $d/150$) and AISC (2016b) (i.e., $L/1000$). Similarly, a smaller amplitude of imperfections may be used in more slender cross-sections.

Prior FE studies on steel columns that utilized stocky cross-sections (Newell and Uang 2006; Elkady and Lignos 2012) suggest that initial residual stresses have a minor effect on the hysteretic behavior of steel columns. This assumption implies that the Wagner coefficient is zero (Trahair 1993); thus, there should not be expected much of a torsional stiffness loss of the member due to residual stresses. This assumption is not valid for deep and slender cross-sections because it yields erroneous residual stress distributions along their web (Sousa and Lignos 2017). Referring to Fig. 2d, the residual stress distribution proposed by Young (1971) is recommended for deep and slender cross-sections (Sousa and Lignos 2017). This distribution is adopted for the purposes of the finite element model proposed herein.

Finite Element Modeling Validation

The proposed FE modeling approach is validated with experimental data from a full-scale test program, recently conducted by the authors (Elkady and Lignos 2018). This program utilized

600mm deep (i.e., W24) cross-sections. Figure 3 shows sample comparisons between the measured cyclic response and the FE simulation predictions in terms of the normalized end moment-rotation and axial shortening-rotation relations for selected column specimens. These represent columns with different cross-sections and end boundary conditions that were subjected to various lateral loading histories coupled with different compressive axial load ratios, P/P_y, where P_y is the measured axial yield strength. Note that P_y is always larger than P_{CL} (as per ASCE 41-13) for a given column cross-section geometry. However, a comparison between the two terms cannot be directly established because their relationship depends on both the cross-section geometry and member length that could vary. Referring to Fig. 3(*top*), the deduced moment-rotation relation is predicted fairly well based on the proposed FE modeling approach including the onset and progression of local and member geometric instabilities. In particular, the associated relative error between the predicted and measured column flexural capacity did not exceed 10% throughout the entire loading history. Referring to Fig. 3 (*bottom*), the proposed FE model was able to accurately capture the column axial shortening up to 4% drift. At larger drift amplitudes, the relative error between the predicted FE simulations and the experimental results was less than 20%.

Figure 4 demonstrates a relatively good agreement between the predicted versus observed deformation profiles at selected lateral drift amplitudes in both the strong- and weak-axis orientation for various specimens. Deep wide flange steel columns are susceptible to twisting and out-of-plane deformations (Elkady and Lignos 2017, 2018; Ozkula et al. 2017). Referring to Figs. 5a and 5b, the FE modeling approach successfully captured these deformations regardless of the cross-section geometry and/or the employed boundary conditions. Figure 5c shows sample comparisons of the measured and predicted longitudinal strain versus chord-rotation, at the center of the flange and 1300mm away from the column base, of one of the tested specimens. Although the reliability of the strain measurements becomes questionable after the onset of yielding, the comparisons suggest that the simulated and measured plastic strains are very comparable.

While the non-uniqueness of the material model parameter fitting does not significantly affect the predicted global force-deformation quantities (Cooke and Kanvinde 2015), the proposed FE modeling approach should be further validated if the intent of a modeler is to assess extreme strain-based limit states (e.g., fracture). In this case, the prediction accuracy of internal plastic strains becomes critical due to non-uniqueness. This is outside the scope of the present work.

In brief, the comparisons between the FE simulations and the experimental results suggest that the proposed FE model adequately predicts the hysteretic behavior of wide-flange steel columns under multi-axis cyclic loading. A number of other validation studies are also presented in detail in Elkady (2016) by employing the modeling assumptions proposed in this paper.

Parametric Simulations

Range of Investigated Cross-Sections

Several untested configurations were investigated through parametric simulations. These include a "simulation-matrix" of 53 wide-flange cross-sections. Both shallow (i.e., W12 to W14) and deep (i.e., W16 to W36) cross-sections are employed as shown in Fig. 6. that summarizes their corresponding web and flange local slenderness ratios. The web and flange λ_{hd} compactness limits according to AISC (2016a) are superimposed in the same figure. To better facilitate the interpretation of the FE results, the 53 cross-sections are divided into four sets based on their web and flange slenderness ratios (i.e., total of eight sets). In brief, the majority of the selected cross-sections are highly ductile, λ_{hd} according to the ANSI/AISC 341-16 (AISC 2016a). The rest of the cross-sections are moderately ductile, λ_{md} as per AISC (2016a). The investigated cross-sections have a member slenderness, L_b/r_y, ranging from 38 to 115. The range of employed column cross-sections is deemed to be representative of those found in modern and existing steel frame buildings designed in highly seismic regions (NIST 2010; Zareian et al. 2010; Bech et al. 2015; Elkady and Lignos 2015b).

Employed Lateral Loading Protocols

The parametric simulations involve three lateral loading protocols. A monotonic; such that each member's monotonic backbone curve can be determined. A symmetric cyclic protocol (Clark et al. 1997) as shown in Fig. 7a, which has been routinely used in prior experimental studies (FEMA 2000). A collapse-consistent protocol (Suzuki and Lignos 2014) as shown in Fig. 7b. This protocol is representative of seismic events with low probability of occurrence in which a building experiences asymmetric lateral loading that is characterized by few inelastic small amplitude cycles followed by large monotonic pushes (i.e., "ratcheting") (Krawinkler 2009; Lignos et al. 2011; Suzuki and Lignos 2014).

The lateral loading protocols are coupled with five levels of constant compressive axial load ratios: 0%, 20%, 35%, 50% and 75% of P_y. These loading conditions are representative of interior steel MRF columns that typically experience fairly small axial load demand fluctuations due to dynamic overturning moments. The axial load variation is more evident in end columns. However, experimental evidence (Suzuki and Lignos 2014, 2017) suggests that although end columns experience higher compressive axial load demands than interior columns during ground motion reversals at which the transient axial load amplifies the gravity-induced compressive load component, they still experience 6 to 7 times less axial shortening compared to interior columns within the same steel MRF bay. The reason is that end columns also experience appreciable tensile axial load in the opposite loading direction resulting into local buckling straightening; thus, the focus of this paper is on the hysteretic response of interior steel columns. Furthermore, although P/P_y > 0.3 is not typically seen in modern steel MRFs (Suzuki and Lignos 2014), it is often common in existing steel MRFs that utilize stocky members (Bech et al. 2015).

Performance Indicators and Implications on Steel Column Stability

Figure 8 shows several indicators to evaluate the steel column stability under multi-axis cyclic loading. These include: the overstrength factor, ρ, calculated as the ratio of the column's maximum flexural strength, M_{max}, to its full plastic strength, M_p; the achieved rotation capacities based on a first-cycle envelope curve (e.g., $\theta_{80\%Mmax}$, see Fig. 8a) that can be directly compared with the current ASCE 41-13 (ASCE 2014) nonlinear modeling recommendations for steel columns; the unloading stiffness deterioration at a given chord-rotation, K_θ, (see Fig. 8a) that is strongly related to the column out-of-plane deformation, Δ_{OP}, near the plastic hinge zone (see Fig. 8b); the column axial shortening, Δ_{axial} (see Fig. 8b); the column plastic hinge length, L_{PH} (see Fig. 8b); and the lateral stability bracing force demands, P_{brace}, that strongly influence the steel column stability (see Fig. 8b).

Column Flexural Capacity

Figures 9a and 9b show the dependence of the overstrength factor, ρ, on the cross-section web slenderness. The plotted FE results are based on columns subjected to a symmetric loading protocol. Referring to Fig. 9a, all the columns reached their full plastic strength M_p for P/P_y=0.2. In particular, steel columns with stocky cross-sections (i.e., set W1 and similarly F1) developed, on average, an overstrength of 1.5. This is attributed to the steel material cyclic hardening prior to the onset of local buckling (i.e., local buckling occurring at drifts > 7%). This is consistent with experimental findings by Newell and Uang (2006). On the other hand, steel columns with cross-sections close to the λ_{hd} limits (i.e., set W3 and similarly F3) developed an average overstrength of 1.08. The observed column overstrength is strongly dependent on the applied compressive axial load ratio that has a profound influence on M_{max}. In particular, Fig. 9b shows that steel columns subjected to a symmetric cyclic loading history coupled with $P/P_y = 0.5$ developed, on average, 35% less overstrength compared to those subjected to $P/P_y = 0.2$.

Figure 9c shows the influence of the web slenderness ratio on the column overstrength based on the symmetric protocol (ρ_{SYM}) over that based on the collapse-consistent protocol (ρ_{CPS}) for $P/P_y = 0.2$. In most cases, the employed lateral loading protocol does not practically influence the observed column overstrength. Only columns with stocky cross-sections (i.e., set W1) subjected to a symmetric loading protocol developed 20% higher overstrength compared to those subjected to a collapse-consistent protocol. This is attributed to the fact that these cross-sections only buckle at very large lateral drift demands (Newell and Uang 2006); and the fact that they are subjected to the large number of small-drift amplitude cycles included in the symmetric protocol. These observations hold true regardless of the employed compressive axial load ratio. The overstrength factor, ρ due to cyclic hardening is dependent on the compressive axial load applied to the respective column and should be considered in the strong-column/weak beam ratio check as per AISC (2016a) and CSA (2009).

Column Rotation Capacity and Comparison with ASCE 41-13 Nonlinear Provisions

Figure 10 shows the achieved column chord-rotation at which 80% M_{max} is reached ($\theta^{SYM-20}_{80\% Mmax}$) versus h/t_w. The results are based on columns subjected to the symmetric loading protocol coupled with P/P_y=0.2. Steel columns with cross-sections in the range $32.5 \leq h/t_w \leq 43$ and $5.5 \leq b_f/2t_f \leq 7$ (i.e., sets W3 and F3) reached 80% M_{max} at an average drift ratio of 2.5%. To put this into perspective, the AISC (2016a) seismic provisions specify that the flexural resistance of steel beams in fully restrained beam-to-column connections, shall not be less than 80% M_p of the connected steel beam after completing one cycle at 4% rads based on the symmetric cyclic loading protocol (i.e., $\theta_{80\%Mp} \geq$ 4% rads). First-story interior MRF columns subjected to a compressive axial load of 20% P_y satisfy this criterion only if a reduction to about two-thirds of the current compactness limit for highly ductile members is employed in the design process. However, it should be acknowledged that the behavior of steel columns is not directly analogous with that of steel beams due to notable differences in their boundary conditions, the moment gradient and the associated inelastic seismic demands that they experience during an earthquake.

The $\theta_{80\%Mmax}$ is based on the first-cycle envelope, which is loading-history dependent. Figure 10b shows the ratio of the achieved $\theta_{80\%Mmax}$ based on the symmetric protocol (i.e., $\theta_{80\%Mmax}^{SYM-20}$) over that achieved based on a collapse-consistent protocol (i.e., $\theta_{80\%Mmax}^{CPS-20}$). In both cases, a $P/P_y = 0.2$ is considered. The results suggest that steel columns subjected to a symmetric loading history achieve roughly a 50% smaller plastic rotation capacity compared to those subjected to a collapse-consistent loading history. This difference becomes minimal at story-drift ratios of 3% or less. This is consistent with prior experimental studies that assessed the effect of loading sequence on the column hysteretic behavior (Suzuki and Lignos 2015; Elkady and Lignos 2018).

The FE simulations offer the opportunity to assess the ASCE/SEI 41-13 (ASCE 2014) nonlinear modeling provisions for steel columns. Of interest are the plastic rotation parameters "*a*" (measured at 80% M_{max}) and "*b*" (measured at 0% M_{max}) of the ASCE/SEI 41-13 cyclic backbone curve as defined in Fig. 11a. Figures 11b and 11c compare the ASCE/SEI 41-13 pre- and post-capping plastic rotations, "*a*" and "*b*", respectively, with the corresponding FE simulation values (noted as a_{FEA} and b_{FEA}). This comparison is established for a range of axial load ratios. Referring to Figs. 11b and 11c, the wide scatter is attributed to the dependence of "*a*" and "*b*" on the member slenderness, L_b/r_y (L_b is the laterally unbraced length and r_y is the weak-axis radius of gyration) and h/t_w, in addition to the axial load ratio, P/P_y (Hamburger et al. 2016; Hartloper and Lignos 2017). Figure 11b suggests that steel columns with stocky cross-sections (i.e., sets W1, F1), subjected to high axial load ratios (i.e., $P/P_{CL} \geq 0.5$), develop an appreciable plastic deformation capacity. Therefore, they do not seem to be force-controlled elements. On the other hand, columns that experience compressive axial loads due to gravity loading larger than 60% P_y (≈ 80% P_{CL}) should be treated as force-controlled elements.

Column Axial Shortening

Figures 12a and 12b show the column axial shortening, Δ_{axial} with respect to the web slenderness ratio, measured at the 2% drift (i.e., representative of design-basis seismic events) based on a symmetric loading protocol coupled with different P/P_y ratios. Referring to Fig. 12a, at P/P_y=0.2, column set W1 shortened by 0.5% L on average while the least λ_{hd} compact column set W3 shortened, on average, by 1.2% L. At higher axial loads, axial shortening developed rapidly due to the web and flange local buckling progression. These observations demonstrate the strong dependency of column axial shortening on h/t_w and P/P_y.

Referring to Fig. 12c, at a 2% reference drift, columns subjected to a symmetric loading history shortened about two times more than nominally identical columns subjected to a collapse-consistent loading history. This demonstrates the dependency of column axial shortening on the cumulative plastic rotation, $\Sigma\theta_{pl}$, which is defined as the sum of absolute plastic drift excursions following the yield rotation, θ_y, of the respective column. The yield rotation is defined as, $\theta_y = M_p (1-P/P_y) / K_e$; in which, K_e is the initial elastic stiffness of the member due to flexural and shear deformations (see Fig. 8a).

MacRae et al. (1990) proposed an empirical formula (Eq. (3)) to predict Δ_{axial} as a function of $\Sigma\theta_{pl}$, the applied axial load ratio, P/P_y, the column plastic hinge length, L_{PH} and the web-to-gross area ratio, A_w/A.

$$\Delta_{axial} = 44.6 \frac{P}{2.54P_y} \frac{A}{A_w} L_{PH} \Sigma\theta_H \qquad \text{for } \frac{P}{P_y} \leq \frac{2.54A_w}{A} \tag{3}$$

$$= 44.6 L_{PH} \Sigma\theta_H \qquad \text{for } \frac{P}{P_y} > \frac{2.54A_w}{A}$$

Equation (3) assumes a linear relationship between Δ_{axial} and $\Sigma\theta_H$. However, this relation is exponential at large drifts due to the excessive web local buckling progression. This can be inferred from Fig. 13a for two of the column specimens tested recently by Elkady and Lignos (2018) at characteristic cumulative plastic rotations (i.e., $\Sigma\theta_{pl}$ = 0.10, 0.25, 0.50). Both specimens had fixed-flexible boundary conditions. Superimposed in the same figure are the calculated Δ_{axial} values based on Eq. (3). Referring to Fig. 13a, Eq. (3) is only valid for story-drift ratios up to 2% ($\approx \Sigma\theta_{pl}$ < 0.25 rads) in which Δ_{axial} is still linearly dependent on $\Sigma\theta_{pl}$.

To improve the accuracy of Eq. (3), a multiple regression is conducted based on the predictive model shown in Eq. (4) to estimate Δ_{axial} based on the FE simulations. The selected variables, $\Sigma\theta_{pl}$, h/t_w, and P/P_y, are found to be statistically significant at the 95% level. For this purpose, a standard *t-test* and *F-test* were conducted. The quality of the regression model is evaluated based on the conditions of the Gauss-Markov theory (Chatterjee and Hadi 2015) including that the mean of the residuals is equal to zero, no correlation is present among the residuals and the residuals have a constant variance. For more details, the reader is referred to Chatterjee and Hadi (2015).

$$\Delta_{axial}\ [\mathrm{mm}] = 13.62\Sigma\theta_{pl}^{\ 1.596}\left(\frac{h}{t_w}\right)^{0.769}\left(1-\frac{P}{P_y}\right)^{-1.819}, \text{(COV=0.281, } R^2\text{=0.873)} \tag{4}$$

Equation (4) is applicable for the following range of predictors: $\Sigma\theta_{pl} \leq 1.0$ rads, $11.1 \leq h/t_w \leq 57.5$, and $0.0 \leq P/P_y \leq 0.75$. Figure 13b shows the scatter of the Δ_{axial} values predicted by Eq. (4) compared to those measured from the FE simulations, indicating a relatively good match. This is also inferred from the corresponding coefficient of determination, $R^2 = 0.873$ and the coefficient of variation $COV = 0.281$. Figure 13a also suggests that Eq. (4) predicts the column axial shortening for the selected experiments reasonably well regardless of $\Sigma\theta_{pl}$.

Elkady and Lignos (2018) found that if the column axial shortening exceeds 1% L, then out-of-plane deformations near the column plastic hinge region are triggered. If the current CAN/CSA S16-09 axial load limit is imposed (i.e., 30% P_y) into Eq. (4), then cross-sections with $h/t_w \leq 37$ can only be utilized if Δ_{axial} is limited to 1% L. The preceding web slenderness ratio corresponds roughly to a 2/3 reduction of the current AISC (2016a) limit for highly ductile members. Alternatively, if a designer choses a cross-section with a $h/t_w \leq \lambda_{hd}$ as per AISC (2016a), then Eq. (4) suggests that the allowable compressive axial load demands on first-story interior columns due to gravity cannot exceed 15% P_y.

For the range of data explored in this paper, it was found that a simple modification to the current AISC 341-16 compactness limit for highly ductile members by 2/3 is suffice to limit column axial shortening to 1% of the respective member length and achieve a maximum of 20% flexural strength reduction at a 4% chord rotation. In this context, it was found that the member slenderness L_b/r_y is somewhat important but only at story drift ratios larger than 3%. Depending on the employed performance objective criteria, alternative expressions may be used for the same purpose such as those proposed by Fogarty et al. (2017) and Wu et al. (2018).

Unloading Stiffness Deterioration due to Geometric Instabilities

Recent experiments conducted by the authors (Elkady and Lignos 2018) suggest that column local buckling is typically followed by out-of-plane deformations, Δ_{OP}, near the column plastic hinge region. These deformations mainly control the unloading stiffness deterioration of the column. Unloading stiffness deterioration due to member instabilities can influence the global stability of steel MRFs at seismic intensities associated with low-probability of occurrence seismic events. Deep columns with member slenderness ratios, L_b/r_y >80 are prone to such failure modes at story drift ratios larger than 3% (Zhang and Ricles 2006; Ozkula et al. 2017; Elkady and Lignos 2018). Accordingly, the unloading stiffness is quantified and assessed.

Figure 14 shows the normalized Δ_{OP}, measured at the 2% drift amplitude versus h/t_w. At P/P_y=20%, highly ductile column cross-sections develop a Δ_{OP} < 1% L (see Fig. 14a). Referring to Fig. 14b, if the current CAN/CSA S16-09 axial load limit of 30% P_y is imposed, columns that employ cross-sections with h/t_w < 32 would develop a Δ_{OP} less than 1% L. This is consistent with earlier observations on the dependence of the column axial shortening on h/t_w and P/P_y.

Figure 15 shows the normalized unloading stiffness $K_{2\%}/K_e$, at a reference lateral drift of 2% versus L_b/r_y for selected P/P_y ratios. Referring to Fig. 15a, columns that utilize stocky cross-sections (i.e., sets W1 and W2) maintain their elastic stiffness (i.e., $K_{2\%}/K_e$ > 0.90) up to 2% drift regardless of L_b/r_y. This is due to the small amount of axial shortening and out-of-plane deformations in this case. Figure 15a suggests that the current CAN/CSA S16-09 (CSA 2009) L_b/r_y limit of about 50~60 for columns in Type-D steel MRFs may be overlay conservative. In particular, steel columns with L_b/r_y < 80, experience less than 50% reduction in their unloading stiffness. On the other hand, based on Fig. 15, it can be inferred that the CAN/CSA S16-09 axial load limit of 30% P_y is rational for Type-D steel MRFs [i.e., equivalent to special moment frames according to

AISC (2016a) and ASCE (2016)]. Interestingly, all the highly ductile cross-sections as per AISC (2016a) maintain at least 50% of their respective K_e at a lateral drift of 2%.

Finally, it is worth noting that although the current seismic provisions for special moment frames (AISC 341-16) and type D ductile moment frames (CSA/S16 09) in North America attempt to limit the inelastic behavior in the beam-to-column web panel zone, this could still occur due to the composite floor slab that increases the flexural capacity of the respective beam and subsequently the panel zone shear demands (Elkady and Lignos 2014). Experiments conducted with deep members and beam-to-column web panel zones that exhibited appreciable inelastic behavior suggest that column twist is considerably reduced in such cases (Zhang and Ricles 2006). This highlights the need for system level experiments that the interactions between deep columns and connections (i.e., beam-to-column and beam-to-column web panel) shall be further studied.

Column Plastic Hinge Length

The column plastic hinge length, L_{PH}, is the distance from the column base to the cross-sectional level with zero plastic strain. Figure 16 shows L_{PH} normalized with respect to the corresponding cross-section depth, d, versus h/t_w. Stocky cross-sections develop a larger plastic hinge length compared to the more slender ones. The former cross-sections are less prone to local buckling than the latter; thus, they can sustain several inelastic cycles prior to plastic strain localization due to local buckling. Notably, the plastic hinge length of columns utilizing highly ductile cross-sections as per AISC (2016a) is on average 2.0 d and 1.6 d for sets W1 and W3, respectively. This is in agreement with the lower-bound L_{PH} values specified by the New Zealand seismic provisions (SNZ 2007). These values are superimposed in Fig. 16 with a dashed line for reference. In particular, SNZ (2007) specifies a minimum L_{PH} of 1.5 d and 1.0 d for category 1 (equivalent to λ_{hd}) and category 3 cross-sections (equivalent to λ_{md}), respectively. Shear stresses due to column twisting also lead to a larger plastic hinge length. In particular, columns with large L_b/r_y tend to develop large L_{PH}. This becomes more evident in columns subjected to bidirectional lateral loading (Elkady and Lignos 2018). Figure 16 also underscores the dependence of L_{PH} on P/P_y. For an axial load increase from 20% P_y (see Fig. 16a) to 50% P_y (see Fig. 16b), the plastic hinge length increased by about 25%. This is attributed to the member second-order moment demands that push the location of the maximum moment away from the column base (Galambos and Surovek 2008).

The L_{PH} affects the steel column stability (SNZ 2007; Peng et al. 2008). In general, it is desirable to have plastic hinges forming at the column ends. If a large plastic hinge length is likely to develop, a designer may consider providing supplementary bracing along the plastified region (SNZ 2007). Kemp (1996) developed an empirical relation for estimating the plastic hinge length in steel beam-columns as follows,

$$L_{PH} = 0.067\left(\frac{60}{\lambda_{eff}}\right)^{1.5} L_i \tag{5}$$

where,

$$\lambda_{eff} = k_f k_w k_d \left(\frac{L_i}{r_{yc}}\right)\gamma\ ,\ \ \gamma = \sqrt{\frac{F_y\ [\mathrm{MPa}]}{250}},\ k_f = \left(\frac{b_f}{2t_f}\right)\frac{\gamma}{9},\ \ k_w = \left(\frac{h_w}{t_w}\right)\frac{\gamma}{70}$$

$k_d = 1.0$, for bare steel beams

in which, L_i is the distance between the inflection point and the column base and r_{yc} is the radius of gyration of the elastic-section under compression (i.e., just before the point that the extreme fibers of the column cross-section reach the yield stress of the respective steel material). This equation is based on 44 wide-flange steel beam monotonic flexural tests and 14 beam-column tests (i.e., monotonic bending and axial force demands). Figure 17a shows a comparison between the predicted plastic hinge length based on Eq. (5) and those measured from the FE parametric study.

Kemp's equation predicts reasonably well the column plastic hinge length for cross-sections that fall within its applicability range (i.e., $5 < b_f/2t_f < 11$ and $39 < h/t_w < 85$). Notably, Kemp's equation seems to highly over predict L_{PH} particularly for stocky cross-sections (i.e., $h/t_w < 32$). However, these cross-sections are outside the applicability of Eq. (5). For this reason, we propose a more general empirical predictive equation. It was found that L_b/r_y, h/t_w and P/P_y are statistically significant to L_{PH} based on a standard *t-test* and *F-test* at a 95% confidence interval. In particular,

$$\frac{L_{PH}}{d} = 1.837\left(\frac{h}{t_w}\right)^{-0.443}\left(\frac{L_b}{r_y}\right)^{0.287}\left(1-\frac{P}{P_y}\right)^{-0.259}, \ (COV{=}0.192,\ R^2{=}0.684) \quad (6)$$

The range of applicability of Eq. (6) is $3.71 \leq h/t_w \leq 57.5$, $39 \leq L_b/r_y \leq 115$, and $0.0 \leq P/P_y \leq 0.75$. Figure 17b shows a comparison between the predicted and measured L_{PH} for the entire dataset. It was also found from the FE parametric simulations that the plastic hinge length is not practically influenced by the employed lateral loading history. It should be noted that rate-effects representative of seismic events were not considered in this case. This issue deserves more attention in future studies.

Lateral Stability Bracing Force Demands

Figure 18 shows the predicted lateral stability bracing force demands, P_{brace} normalized with respect to P_y, versus L_b/r_y, at selected P/P_y ratios. Referring to Fig. 8b, the P_{brace} values refer to the nodal lateral bracing for steel column stability. The FE simulations suggest that there is a strong influence of L_b/r_y on P_{brace}. This finding is confirmed by experimental nodal lateral bracing force demand measurements (Elkady and Lignos 2018) that are superimposed in Fig. 18 for reference.

For columns and beam-to-column joints in Type-D steel MRFs, the CSA (2009) seismic provisions specify a lateral brace axial strength, P_b:

$$P_b = 0.02\ C_f = 0.02\ (1.1\ R_y\ F_{yn}\ A_{comp}) \tag{8}$$

in which, R_y is a factor applied to estimate the probable yield stress (taken as 1.1) and A_{comp}, is the cross-sectional area in compression (see Clause 9.2.5). Similarly, for beam-columns, the ANSI/AISC360-16 (AISC 2016b) specifies a lateral "nodal" brace axial strength, P_{rb}:

$$P_{rb} = 0.01\ P_r + 0.02\ M_r\ C_d\ /\ h_o \tag{9}$$

in which, P_r and M_r are the required axial and flexural strength of the beam-column, respectively, h_o is the distance between flange centroids, and $C_d = 2.0$ for braces closest to the column inflection point. The nodal lateral bracing design forces computed from Eqs. (8) and (9) are superimposed in Fig. 18. It is evident that the stability bracing design requirements overestimate the nodal lateral bracing design forces for steel MRF column stability by a factor of two for member slenderness, $L_b/r_y \geq 60$ regardless of the compressive axial load demands. This is in part associated with the fact that both equations have been derived with the assumption of an infinite number of braces, which is a conservative one for all cases (Geschwindner and Lepage 2013). In addition, Eqs. (8) and (9) do not reflect the apparent dependence of P_{brace} on L_b/r_y. Notwithstanding the limitations in the above equation derivations according to the elastic stability theory (Galambos and Surovek 2008), the current design approach according to the AISC (2016b) specifications is deemed to be safe for columns with $L_b/r_y > 60$ but may be insufficient for $L_b/r_y < 60$ considering that the nodal bracing forces may amplify for real columns with initial out-of-plumbness as seen from the available experimental data (Elkady and Lignos 2018).

Figure 18b also suggests that the stiffness requirement for lateral bracing of steel columns, in accordance with the AISC (2016b) specifications, controls over the strength if $P/P_y > 0.35$. However, this limit is still much larger than the measured nodal stability bracing force demands.

This necessitates a thorough assessment of the lateral stability bracing for beam-columns vis-à-vis the above discussion. This is possibly one of the most important areas of future work.

Summary and Conclusions

Comprehensive parametric finite element (FE) simulations are conducted to study the seismic performance of steel MRF columns and to propose improved recommendations to the current seismic design provisions in North America. This is achieved with a high-fidelity FE modeling approach that was validated with available tests on steel columns subjected to multi-axis cyclic loading. The main findings of this paper are summarized below:

- Modern steel MRF columns (i.e., range of axial load ratios P/P_y~20%), with deep and slender cross-sections, near the compactness limits for highly ductile members (λ_{hd}) as per AISC (2016a) (i.e., 32.5≤ h/t_w ≤43 and 5.5≤ $b_f/2t_f$ ≤7) develop an average overstrength of 1.08. Steel columns that employ stocky cross-sections (i.e., $h/t_w \leq 22$ and $b_f/2t_f \leq 3.9$) develop an average overstrength of 1.50 for the same axial load ratio due to the local buckling delay even at very large lateral drift demands (i.e., 7%). This shows the influence of local slenderness on member overstrength. The column overstrength is reduced by 35%, on average, for P/P_y = 50%, which may reflect the axial load demands in existing tall steel MRFs. The above values do not seem to be influenced by the imposed lateral loading history.
- The plastic deformation capacity of steel columns is strongly dependent on, L_b/r_y, h/t_w and P/P_y. These dependences are not fully reflected in the current ASCE 41-13 (ASCE 2014) nonlinear modeling recommendations. The plastic deformation capacity of steel columns at the bottom-stories of modern steel MRFs can be significantly increased (i.e., limiting the reduction in flexural strength to 20% M_{max} at a reference lateral drift of 2%), if a reduction to about two-thirds of the current λ_{hd} compactness limit as per AISC (2016a) is employed.

- Experiments and FE simulations demonstrate that seismically compact steel columns subjected to $P/P_{CL} \geq 0.5$ develop an appreciable plastic deformation capacity; hence, they may not be force-controlled elements as discussed in ASCE (2014). Instead, it is recommended that this limit is raised to $P/P_y \geq 0.6$.
- The CAN/CSA S16-09 (CSA 2009) limit of P/P_y=0.3 (due to gravity) for columns as part of Type-D Ductile MRFs, is rational and should be incorporated in future versions of the ANSI/AISC 341-16 (AISC 2016a). This reduces the column axial shortening, the plastic hinge length and the magnitude of out-of-plane deformations near the column base.
- An empirical expression is proposed to estimate column axial shortening, Δ_{axial} with respect to h/t_w, P/P_y, and the cumulative plastic rotation, $\Sigma\theta_{pl}$. Unlike prior predictive equations, the proposed expression captures well the exponential increase of Δ_{axial} at drifts larger than 2%. It can also facilitate the effective selection of column cross-sections if a design objective is to limit Δ_{axial}, which is currently not addressed in North American seismic design standards. For instance, if P/P_y is limited to 0.3, only cross-sections with h/t_w < 37 should be utilized (roughly 2/3 of the current λ_{hd} limits) such that Δ_{axial} becomes less than 1% of the member length, L.
- The current CSA (2009) L_b/r_y limit of 60 may be relaxed to 80. Similarly, to control the cyclic deterioration in lateral stiffness, an upper limit of 0.45 may be considered for the torsional slenderness, λ_{LTB} of a steel MRF column. These limits could be adopted in future versions of the ANSI/AISC 341-16 (AISC 2016a) seismic design provisions.
- The lower-bound plastic hinge length, L_{PH} for both highly and moderately ductile steel columns according to the New Zealand seismic provisions (SNZ 2007) is consistent with the ones presented in this paper. A general empirical equation is proposed to predict L_{PH}. This equation extends the

range of applicability of the empirical equation by Kemp (1996) to both highly and moderately compact cross-sections ($3.71 \leq h/t_w \leq 32.5$).

- The safety margin for the lateral stability bracing design force of beam-columns as per CSA (2009) and AISC (2016b) may be insufficient for columns with $L_b/r_y < 60$. On the other hand, the same lateral bracing strength requirements may be overestimating the force demand by a factor of two for steel columns with $L_b/r_y > 60$. Depending on the applied compressive axial load ratio, the lateral bracing due to stiffness may control over the strength requirement of the AISC (2016b) specifications.

It should be stated that the improved seismic design recommendations for steel MRF columns presented herein are based on the specific performance objectives defined by the authors. These recommendations may be modified accordingly by targeting alternative performance objectives.

Acknowledgements

This study is based on work supported by the Swiss National Science Foundation (Award No. 200021_169248). This financial support is gratefully acknowledged. The authors sincerely thank Prof. Charles Clifton from University of Oakland, New Zealand for his valuable assistance to interpret the column plastic hinge lengths according to the New Zealand Standard (SNZ 2007). The authors also thank Mr. Alex Hartloper for his feedback and assistance with multiple regression analysis. Any opinions, findings, and conclusions or recommendations expressed in this paper are those of the authors and do not necessarily reflect the views of sponsors.

References

ABAQUS-FEA/CAE. 2011. Dassault Systemes Simulia Corp., RI, USA. © Dassault Systèmes, 2010.

AISC (2016a). "Seismic provisions for structural steel buildings." *ANSI/AISC 341-16*, Chicago, IL.

AISC (2016b). "Specification for structural steel buildings ".*ANSI/AISC 360-16*, Chicago, IL.

Alpsten, G. A. (1968). "Thermal residual stresses in hot-rolled steel members." *Fritz Engineering Laboratory Report No. 337.3*, Department of Civil and Environmental Engineering, Lehigh University.

ASCE (2014). "Seismic evaluation and retrofit of existing buildings." *ASCE/SEI 41-13*, Reston, VA.

ASCE (2016). "Minimum design loads and asscoiated criteria for buildings and other structures." *ASCE/SEI 7-16*, Reston, VA.

ASTM (2003). "Standard specification for general requirements for rolled structural steel bars, plates, shapes, and sheet piling." *ASTM A6/A6M-04b*, American Society for Testing and Materials, West Conshohocken, PA.

ASTM (2015). "Standard specification for structural steel shapes." *ASTM A992/A992M-11*, ASTM International, West Conshohocken, PA, USA.

Bech, D., Tremayne, B., and Houston, J. (2015). "Proposed changes to steel column evaluation criteria for existing buildings." *Proc., 2nd ATC-SEI Conf. on Improving the Seismic Performance of Existing Building and Other Structures*, Earthquake Engineering Research Institute, San Francisco, CA, USA. DOI: 10.1061/9780784479728.022.

Chatterjee, S., and Hadi, A. S. (2015). *Regression analysis by example*, Fifth Edition, John Wiley & Sons.

Chen, Y. Y., Niu, L., and Cheng, X. (2014). "Hysteretic behaviour of H steel columns with large width-thickness ratios under bi-axis moments." *Proc., 10th National Conf. on Earthquake Eng.*, Earthquake Engineering Research Institute, Anchorage, AK, USA.

Cheng, X., Chen, Y., and Pan, L. (2013). "Experimental study on steel beam–bolumns composed of slender H-sections under cyclic bending." *J. of Constructional Steel Research*, 88, 279-288. DOI: 10.1016/j.jcsr.2013.05.020.

Clark, P., Frank, K., Krawinkler, H., and Shaw, R. (1997). "Protocol for fabrication, inspection, testing, and documentation of beam-column connection tests and other experimental specimens." *Report No. SAC/BD-97/02*, SAC Joint Venture, Sacramento, CA, USA.

Cooke, R. J., and Kanvinde, A. M. (2015). "Constitutive parameter calibration for structural steel: Non-uniqueness and loss of accuracy." *J. of Constructional Steel Research*, 114, 394-404, DOI: 10.1016/j.jcsr.2015.09.004.

CSA (2009). "Design of steel structures." *CAN/CSA S16-09*, Mississauga, Canada.

Elkady, A. (2016). "Collapse risk assessment of steel moment-resisting frames designed with deep wide-flange columns in seismic regions." *Ph.D. Thesis*, McGill University, Canada.

Elkady, A., and Lignos, D. G. (2012). "Dynamic stability of deep slender steel columns as part of special MRFs designed in seismic regions: Finite element modeling." *Proc., First Int. Conf. on Performance-Based and Life-Cycle Structural Eng.*, Faculty of Construction and Environment and the Research Institute for Sustainable Urban Development, Hong Kong Polytechnic University, Hong Kong, China.

Elkady, A., and Lignos, D. G. (2014). "Modeling of the composite action in fully restrained beam-to-column connections: implications in the seismic design and collapse capacity of steel special moment frames.” *Earthquake Engineering & Structural Dynamics*, 43(13), 1935-1954, DOI: 10.1002/eqe.2430.

Elkady, A., and Lignos, D. G. (2015a). "Analytical investigation of the cyclic behavior and plastic hinge formation in deep wide-flange steel beam-columns." *Bull Earthquake Eng*, 13(4), 1097-1118, DOI: 10.1007/s10518-014-9640-y.

Elkady, A., and Lignos, D. G. (2015b). "Effect of gravity framing on the overstrength and collapse capacity of steel frame buildings with perimeter special moment frames." *Earthquake Engineering & Structural Dynamics*, 44(8), 1289–1307, DOI: 10.1002/eqe.2519.

Elkady, A., and Lignos, D. G. (2017). "Stability Requirements of Deep Steel Wide-Flange Columns under Cyclic Loading." *Proc., ASCE Annual Stability Conference,* American Society of Civil Engineers, San Antonio, Texas, USA.

Elkady, A., and Lignos, D. G. (2018). "Full-scale testing of deep wide-flange steel columns under multi-axis cyclic loading: Loading sequence, boundary effects and out-of-plane brace force demands." *Journal of Structural Engineering*, , 144(2), DOI: 10.1061/(ASCE)ST.1943-541X.0001937.

FEMA (2000). "State of the art report on connection performance." *Report FEMA-355D*, Federal Emergency Management Agency, Washington, DC.

Fogarty, J., Wu, T. Y., and El-Tawil, S. (2017). "Collapse response and design of deep steel columns subjected to lateral displacement." *Journal of Structural Engineering*, 143(9), DOI: 10.1061/(ASCE)ST.1943-541X.0001848.

Galambos, T. V., and Surovek, A. E. (2008). *Structural stability of steel: Concepts and applications for structural engineers*, John Wiley & Sons.

Geschwindner, L. F., and Lepage, A. (2013). "Notes on the nodal and relative lateral stability bracing requirements of AISC 360." *AISC Engineering Journal*, 50(3), 169-179.

Grilli, D., Jones, R., and Kanvinde, A. (2017). "Seismic performance of embedded column base connections subjected to axial and lateral loads." *Journal of Structural Engineering*, 143(5), DOI: 10.1061/(ASCE)ST.1943-541X.0001741.

Gupta, A., and Krawinkler, H. (1999). "Seismic demands for the performance evaluation of steel moment resisting frame structures." *Report No. 132*, The John A. Blume Earthquake Engineering Center, Stanford University, CA.

Hamburger, R. O., Deierlein, G., Lehman, D., Lowes, L. N., Shing, B., Van de Lindt, J., Lignos, D. G., and Hortacsu, A. (2016). "ATC-114 next-generation hysteretic relationships for performance-based modeling and analysis." *Proc., Structural Engineers Association of California Convention*, Maui, Hawai, USA.

Hartloper, A., and Lignos, D. G. (2017). "Updates to the ASCE 41-13 provisions for the nonlinear modeling of steel wide-flange columns for performance-based earthquake engineering." *Proc., 8^{th} European Conf. on Steel and Composite Structures*, Copenhagen, Denmark, 3072-3081.

Inamasu, H., Kanvinde, A., and Lignos, D. G. (2017). "The seismic stability and ductility of steel columns interacting with concrete footings." *Proc., 8^{th} Int. Conf. on Composite Construction in Steel and Concrete*, Jackson, Wyoming, USA.

Kanvinde, A., Grilli, D., and Zareian, F. (2012). "Rotational stiffness of exposed column base connections: Experiments and analytical models." *Jornal of Structural Engineering*, 138(5), DOI: 10.1061/(ASCE)ST.1943-541X.0000495.

Kemp, A. R. (1996). "Inelastic local and lateral buckling in design codes." *Journal of Structural Engineering*, 122(4), 374-382. DOI: 10.1061/(ASCE)0733-9445(1996)122:4(374).

Krawinkler, H. (2009). "Loading histories for cyclic tests in support of performance assessment of structural components." *Proc., 3rd Int. Conf. on Advances in Experimental Structural Engineering*, Pacific Earthquake Engineering Research Center, San Francisco, CA.

Lemaitre, J., and Chaboche, J. L. (1990). *Mechanics of solid materials*, Cambridge University Press, Cambridge, UK.

Lignos, D. G., Cravero, J., and Elkady, A. (2016). "Experimental investigation of the hysteretic behavior of wide-flange steel columns under high axial load and lateral drift demands." *Proc., 11th Pacific Structural Steel Conference*, China Steel Construction Society, Shanghai, China.

Lignos, D. G., Krawinkler, H., and Whittaker, A. S. (2011). "Prediction and validation of sidesway collapse of two scale models of a 4-story steel moment frame." *Earthquake Engineering & Structural Dynamics*, 40(7), 807-825, DOI: 10.1002/eqe.1061.

MacRae, G. A., Carr, A. J., and Walpole, W. R. (1990). "The seismic response of steel frames." *Report No. 90-6*, Department of Civil Engineering, University of Canterbury, New Zealand.

Nakashima, M., Takanashi, K., and Kato, H. (1990). "Test of steel beam-columns subject to sidesway." *Journal of Structural Engineering*, 116(9), DOI: 10.1061/(ASCE)0733-9445(1990)116:9(2516).

Newell, J. D., and Uang, C.-M. (2006). "Cyclic behavior of steel columns with combined high axial load and drift demand." *Report No. SSRP-06/22*, Department of Structural Engineering, University of California, San Diego.

NIST (2010). "Evaluation of the FEMA P695 methadology for quantification of building seismic performance factors." National Institute of Science and Technology, *NIST GCR 10-917-8*, NEHRP consultants Joint Venture, Redwood City, California.

Ozkula, G., Harris, J., and Uang, C. M. (2017). "Observations from cyclic tests on deep, wide-flange beam-columns." *AISC Engineering Journal*, 54(1), 45-61.

Peng, B. H. H., MacRae, G. A., Walpole, W. R., Moss, P., Dhakal, R. P., Clifton, C., and Hyland, C. (2008). "Location of plastic hinges in axially loaded steel members." *J. of Constructional Steel Research*, 64(3), 344-351. DOI: 10.1016/j.jcsr.2007.08.004.

Popov, E. P., Bertero, V. V., and Chandramouli, S. (1975). "Hysteretic behavior of steel columns." *Report No. EERC 75-11*, Earthquake Engineering Research Center, University of California.

SNZ (2007). "Steel structures standard." *NZS 3404: 2007*, Standards New Zealand, Wellington, New Zealand.

Sousa, A. A., and Lignos, D. G. (2017). "Residual stress measurements of european hot-rolled i-shaped steel profiles." *EPFL-REPORT-231302*, Ecole Polytechnique Federale de Lausanne, Switzerland. https://infoscience.epfl.ch/record/231302.

Stoakes, C. D., and Fahnestock, L. A. (2016). "Strong-axis stability of wide flange steel columns in the presence of weak-axis flexure." *Journal of Structural Engineering*, 142(5), DOI: 10.1061/(ASCE)ST.1943-541X.0001448.

Suzuki, Y., and Lignos, D. G. (2014). "Development of loading protocols for experimental testing of steel columns subjected to combined high axial load and lateral drift demands near collapse." *Proc., 10th National Conf. on Earthquake Eng.*, Earthquake Engineering Research Institute, Anchorage, AK, USA. DOI: 10.4231/D3M32N99R.

Suzuki, Y., and Lignos, D. G. (2015). "Large scale collapse experiments of wide-flange steel beam-columns." *Proc., 8th Int. Conf. on Behavior of Steel Structures in Seismic Areas*, Tongji University, Shanghai, China.

Suzuki, Y., and Lignos, D. G. (2017). "Collapse behavior of steel columns as part of steel frame buildings: Experiments and numerical models." *Proc., 16th World Conf. on Earthquake Engineering*, International Association for Earthquake Engineering, Santiago, Chile.

Trahair, N. S. (1993). *Flexural-torsional buckling of structures*, CRC Press.

von Mises, R. (1913). "Mechanik der festen körper im plastisch-deformablen zustand." *Nachrichten von der Gesellschaft der Wissenschaften zu Göttingen, Mathematisch-Physikalische Klasse*, 1, 582-592.

Wu, T.-Y., El-Tawil, S., and McCormick, J. (2018). "Highly ductile limits for deep steel columns." *Journal of Structural Engineering*, 144(4), 04018016, DOI: 10.1061/(ASCE)ST.1943-541X.0002002.

Young, B. W. (1971). "Residual stresses in hot-rolled sections." *Proc., Int. Colloquium on Column Strength, Int. Association for Bridge and Structural Eng.*, International Association for Bridge and Structural Engineering, Zurich, Switzerland, 25-38.

Zareian, F., Lignos, D. G., and Krawinkler, H. (2010). "Evaluation of seismic collapse performance of steel special moment resisting frames using FEMA P695 (ATC-63) methodology." *Proc., ASCE Structures Congress*, American Society of Civil Engineers, Orlando, FL, USA, 1275-1286.

Zhang, X., and Ricles, J. M. (2006). "Experimental evaluation of reduced beam section connections to deep columns." *Journal of Structural Engineering*, 132(3), 346-357, DOI: 10.1061/(ASCE)0733-9445(2006)132:3(346).

List of Figures

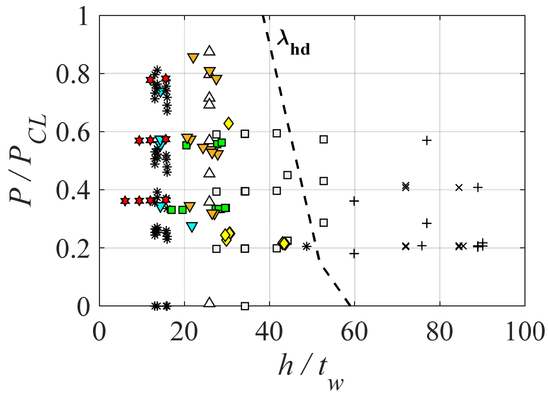

(a)

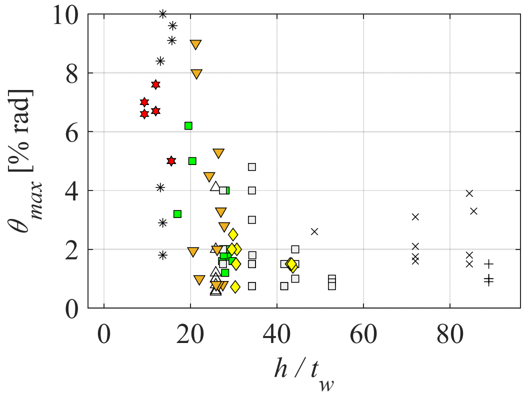

(b)

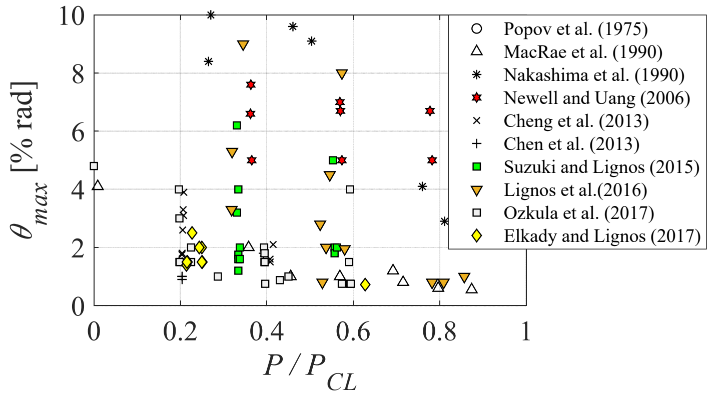

(c)

Fig. 1. Distribution of θ_{max} with respect to web slenderness and axial load ratio for available experimental data on wide flange steel columns

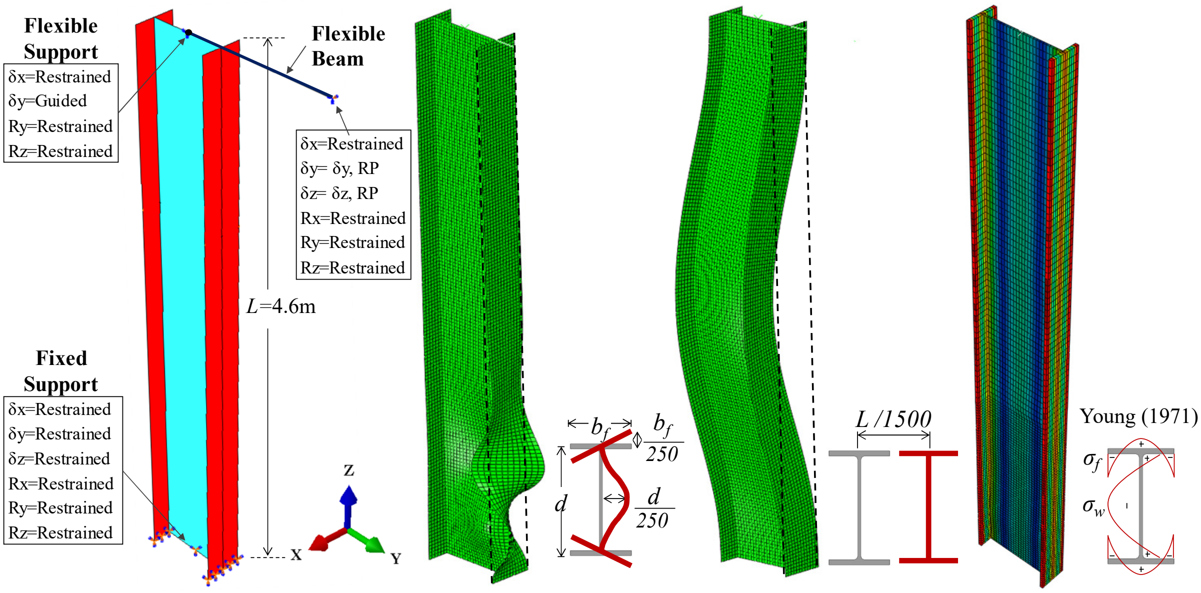

666 (a) Boundary conditions (b) Local buckling mode (c) Global buckling mode (d) Residual stress profile

667 **Fig. 2.** Finite element model specifics for wide-flange steel columns

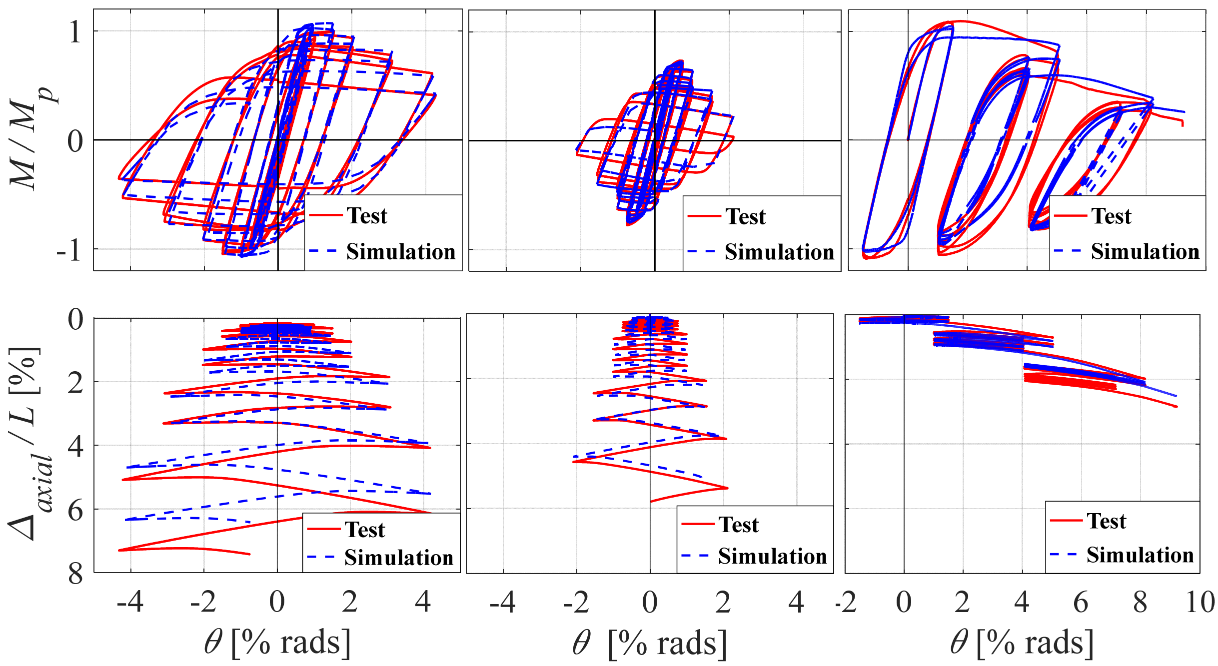

(a) W24x146, P/P_y=0.2 Unidirectional symmetric

(a) W24x146, P/P_y=0.5 Unidirectional symmetric

(c) W24x84, P/P_y=0.2 Bidirectional collapse-consistent

Fig. 3. Comparison between simulated and experimental results: moment-rotation (*top*) and axial shortening-rotation (*bottom*) [data from Elkady and Lignos (2018)]

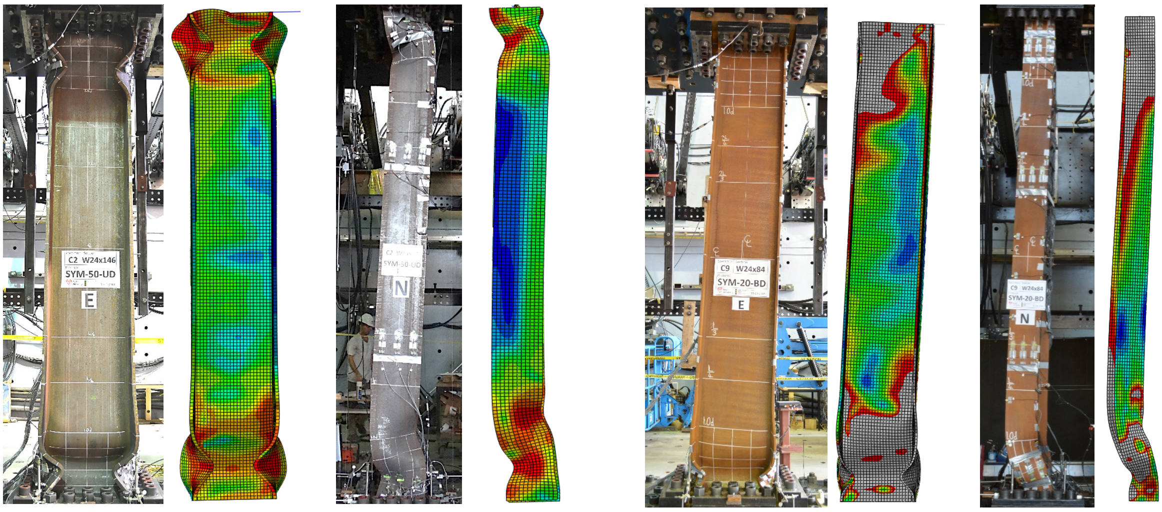

(a) Specimen C2, W24x146, P/P_y=0.5
Unidirectional Symmetric Cyclic

(b) Specimen C2, W24x146, P/P_y=0.2
Bidirectional Symmetric Cyclic

Fig. 4. Comparison between simulated and experimentally obtained deformation profiles [data from Elkady and Lignos (2018)]

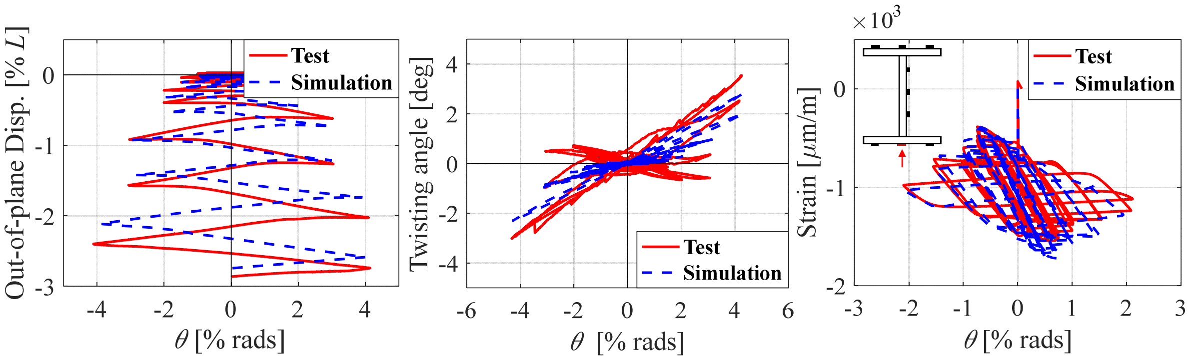

(a) Spec. C9, 1.3m from base (b) Spec. C1, 1.3m from base (c) Spec. C2, 1.3m from base

Fig. 5. Comparison between simulated and experimental results: (a) out-of-plane displacement, (b) twisting angle, and (c) flange longitudinal strain, [data from Elkady and Lignos (2018)]

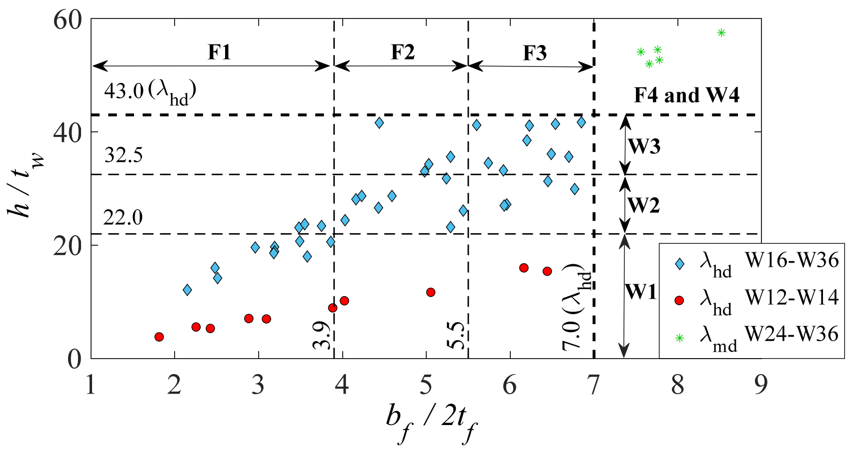

Fig. 6. Selected cross-sections for finite element parametric simulations

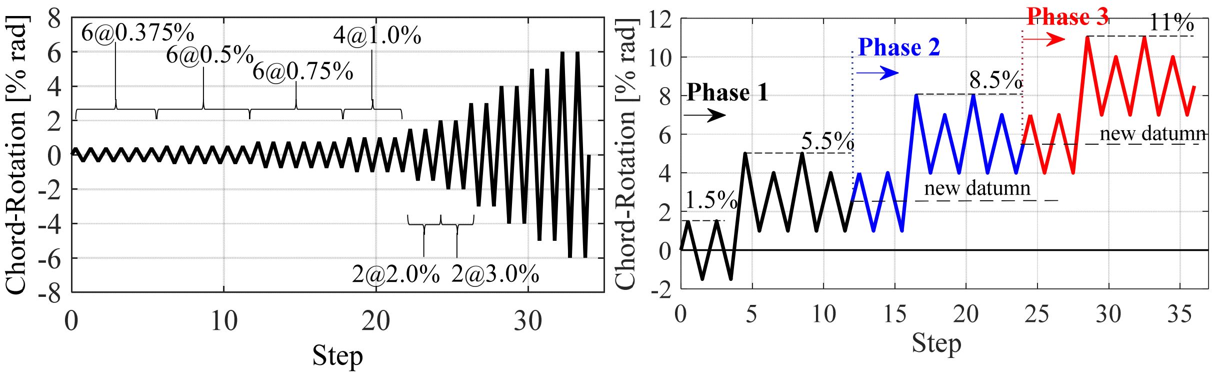

(a) Symmetric protocol (b) Collapse-consistent protocol

Fig. 7. Employed lateral loading protocols

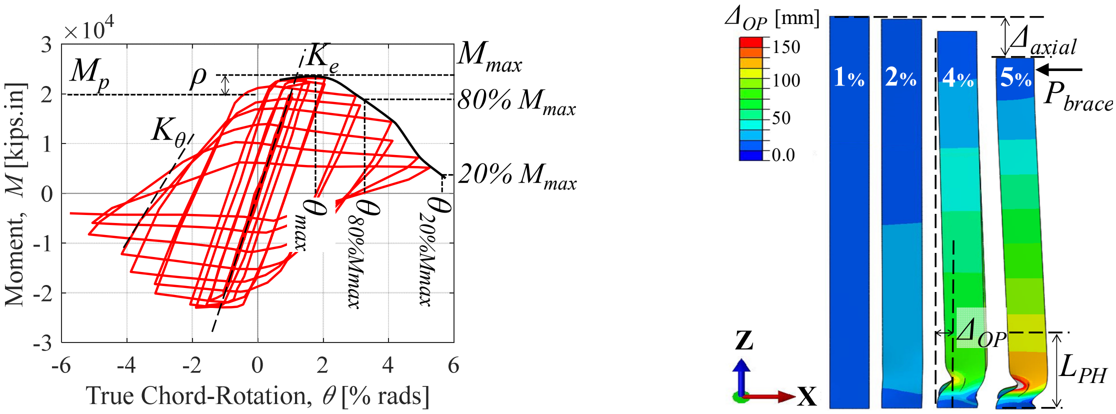

(a) end-moment versus chord-rotation (b) global deformation profile

Fig. 8. Damage progression performance indicators for wide-flange steel columns

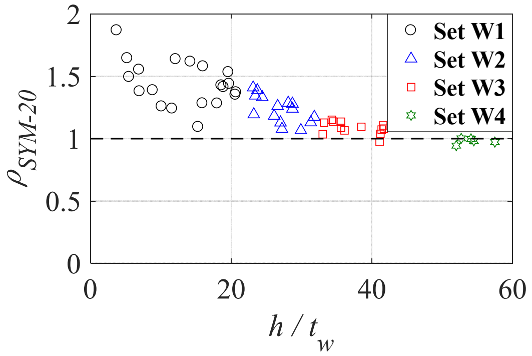

(a) SYM lateral loading coupled with P/P_y=0.2

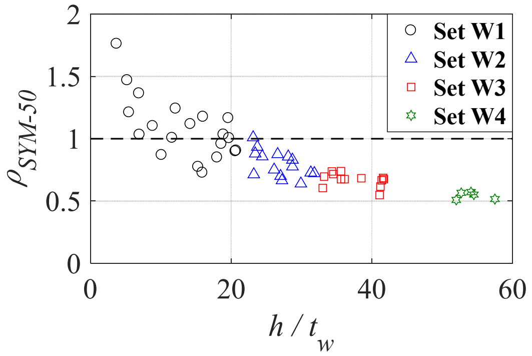

(b) SYM lateral loading coupled with P/P_y=0.5

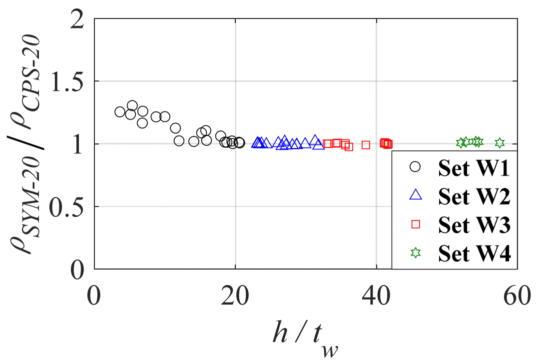

(c) Dependence of column overstrength on lateral loading history

Fig. 9. Dependence of column overstrength on web slenderness ratio and loading history

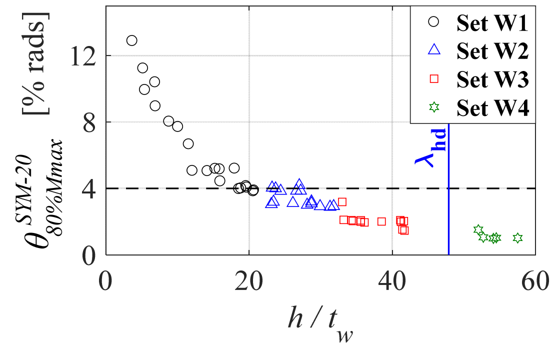

(a)

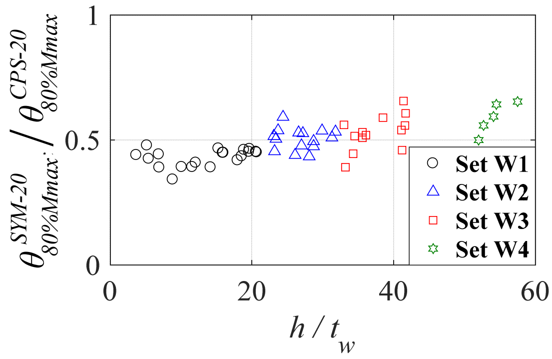

(b)

Fig. 10. (a) Rotation capacity, $\theta_{80\%Mmax}^{SYM-20}$, versus web slenderness ratio (symmetric protocol, P/P_y=0.2); (b) ratio of $\theta_{80\%Mmax}^{SYM-20}$ to $\theta_{80\%Mmax}^{CPS-20}$ versus web slenderness ratio

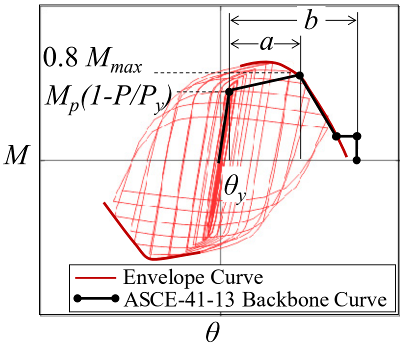

(a)

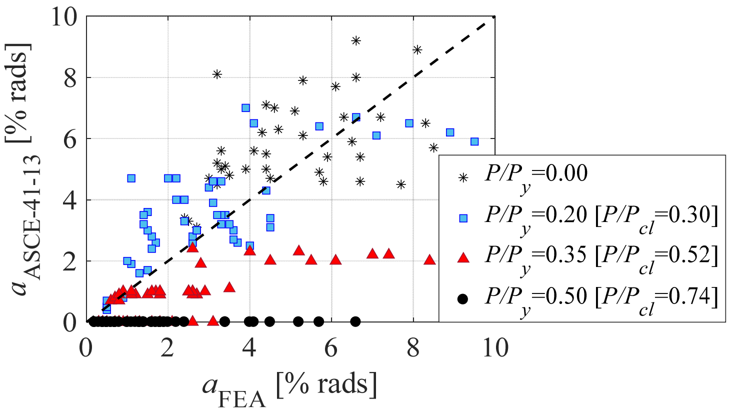

(b)

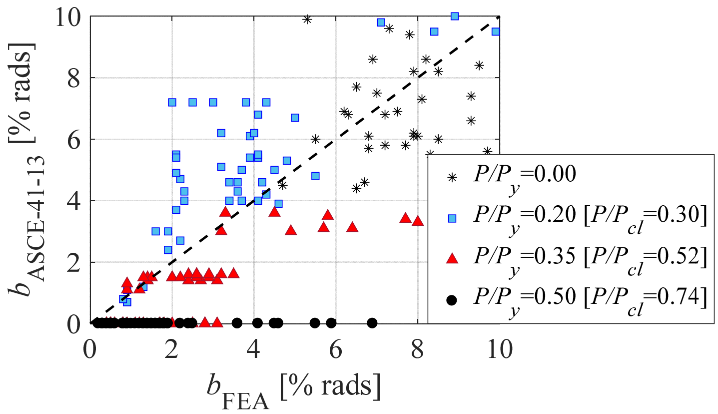

(c)

Fig. 11. Plastic rotation parameters "*a*" and "*b*" based on ASCE 41-13 and FE simulations

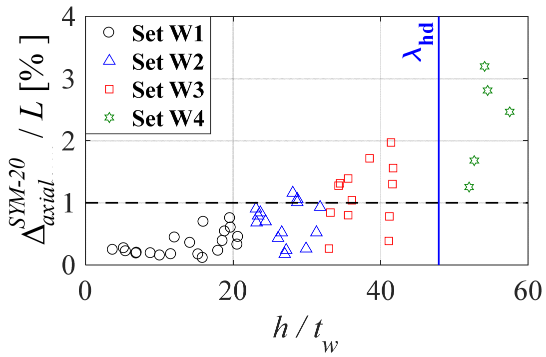

(a) P/P_y=0.2

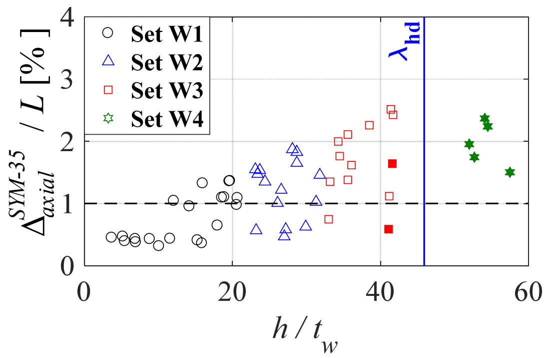

(b) P/P_y=0.35

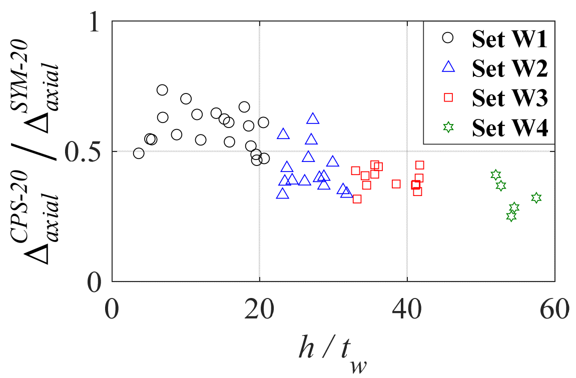

(c) Dependence of column axial shortening on the lateral loading history

Fig. 12. Column axial shortening measured at 2% lateral drift versus web slenderness ratio

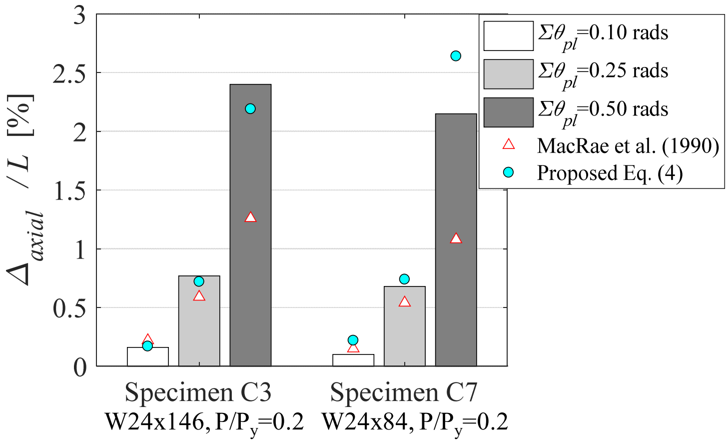

(a)

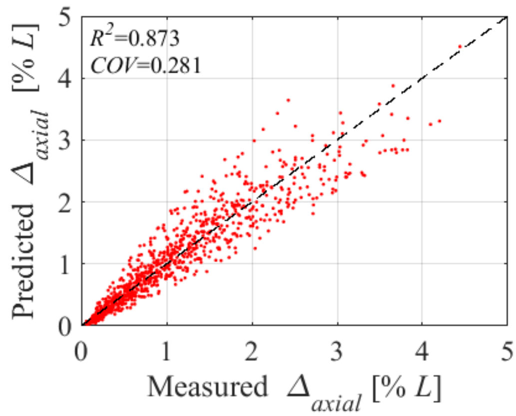

(b)

Fig. 13. Comparison of predicted versus measured normalized column axial shortening

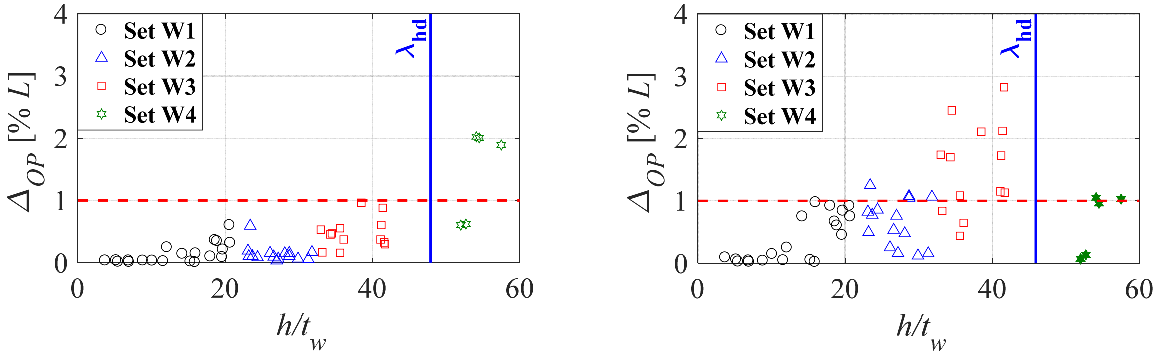

(a) P/P_y=0.2 (b) P/P_y=0.35

Fig. 14. Normalized out-of-plane deformation near the column base at 2% drift versus web slenderness ratio (symmetric loading history)

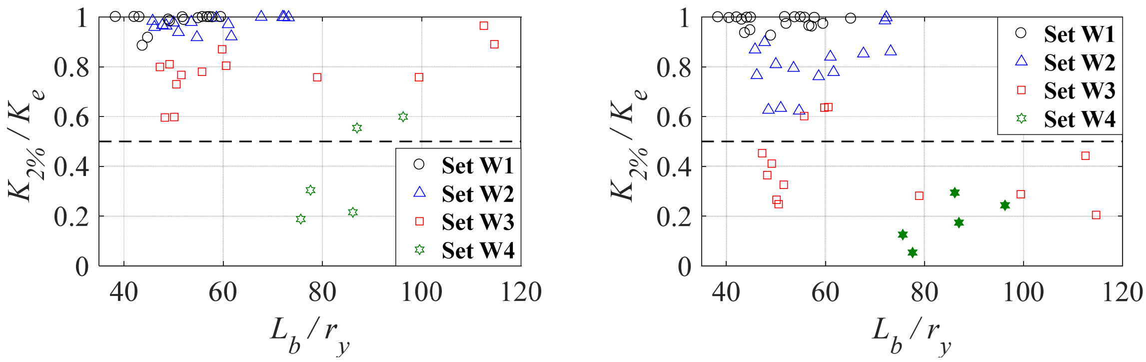

(a) P/P_y=0.2 (b) P/P_y=0.35

Fig. 15. Normalized unloading stiffness measured at 2% drift versus member slenderness ratio, L_b/r_y (symmetric loading history)

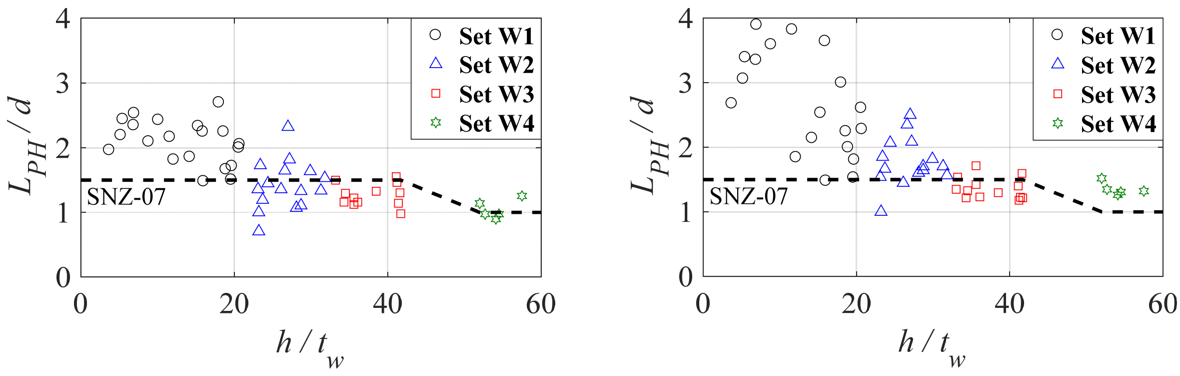

(a) P/P_y=0.2 (b) P/P_y=0.50

Fig. 16. Normalized plastic hinge length versus web slenderness ratio at selected axial load ratios

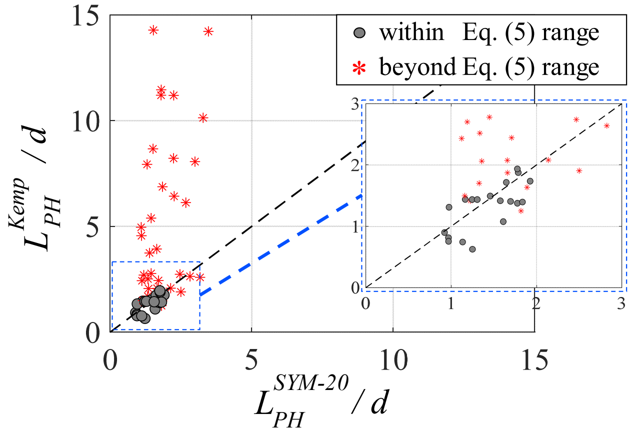

(a) Kemp (1996) empirical equation

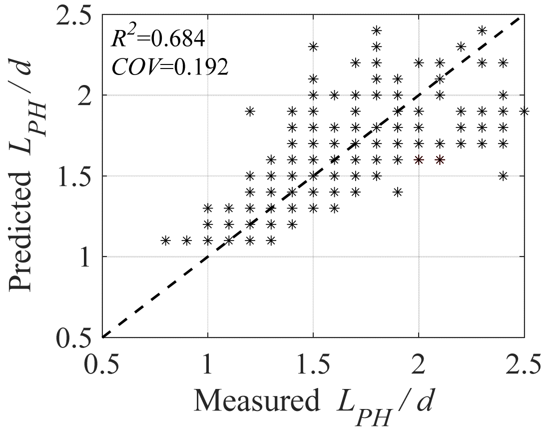

(b) Proposed empirical equation

Fig. 17. Predicted normalized plastic hinge length, L_{PH}/d and comparison with empirical models

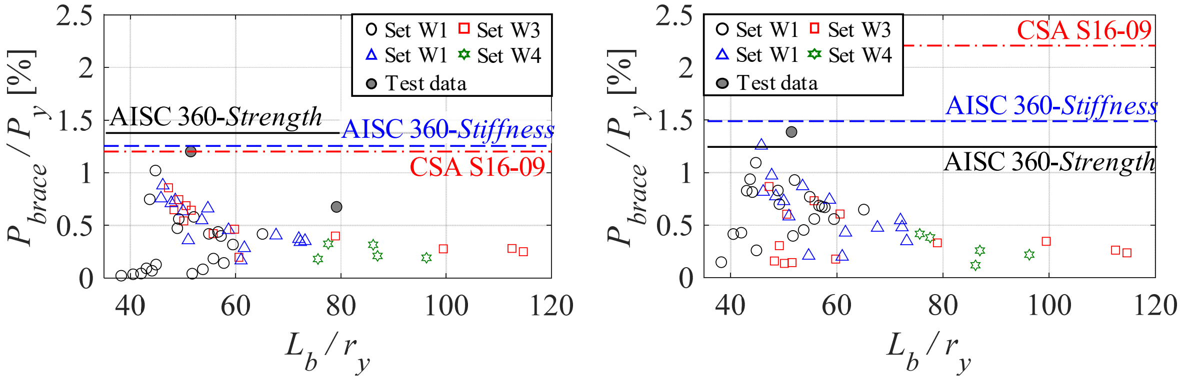

(a) P/P_y=0.2 (b) P/P_y=0.50

Fig. 18. Normalized lateral stability bracing force demands versus member slenderness ratio for columns subjected to a symmetric loading history